Article

A non-enzyme cascaded amplification biosensor based on effective aggregation luminescence caused by disintegration of silver nanoparticles

Weipan Peng, Yi Qin, Wenna Li, Minghui Chen, Dianming Zhou, Hengxuan Li, Jingyu Cui, Jin Chang, Sheng Xie, Xiaoqun Gong, and Ben Zhong Tang

ACS Sens., **Just Accepted Manuscript** • DOI: 10.1021/acssensors.9b02355 • Publication Date (Web): 24 Jun 2020

A non-enzyme cascaded amplification biosensor based on effective aggregation luminescence caused by disintegration of silver nanoparticles

Weipan Peng[1#], Yi Qin[1#], Wenna Li[1], Minghui Chen[1], Dianming Zhou[5], Hengxuan Li[1], Jingyu Cui[1], Jin Chang[1*], Sheng Xie[2*], Xiaoqun Gong[1*], Benzhong Tang[3,4]

[1]School of Life Sciences, Tianjin University and Tianjin Engineering Center of Micro-Nano Biomaterials and Detection-Treatment Technology (Tianjin), Tianjin 300072, China

[2]State Key Laboratory of Chemo/Biosensing and Chemometrics, College of Chemistry and Chemical Engineering, Hunan University, Changsha 410000, China

[3]Department of Chemistry, Department of Chemical and Biological Engineering, Hong Kong Branch of Chinese National Engineering Research Center for Tissue Restoration and Reconstruction, Institute for Advanced Study, Institute of Molecular Functional Materials, The Hong Kong University of Science and Technology, Clear Water Bay, Kowloon, Hong Kong 999077, China

[4]Center for Aggregation-Induced Emission, SCUT-HKUST Joint Research Institute, State Key Laboratory of Luminescent Materials and Devices, South China University of Technology, Guangzhou 510640, China

[5]Department of Toxicology, Tianjin Centers for Disease Control and Prevention, Tianjin 30000, China

[#]Authors who contributed equally to this work.

*Corresponding authors: Xiaoqun Gong, gongxiaoqun@tju.edu.cn

Sheng Xie, shengxie@hnu.edu.cn

Jin Chang, jinchang@tju.edu.cn

Abstract:

Sensitive and portable quantification of biomarkers has particular significance for the monitoring and treatment of clinical diseases. Conventional immunoassays were accustomed to introducing or incorporating enzymes for signal amplification, which commonly suffered from poor stability and inferior tolerance. Herein, we constructed a novel non-enzyme amplification methodology based on fluorogenic Ag^{+}-tetrazolate aggregation coupled with silver corrosion sensitization for biomarkers determination. A significant cascade enhancement strategy was achieved by the valid aggregation luminescence caused by the potent disintegration of silver nanoparticles (AgNPs). Furthermore, the efficient magnetic separation was also combined and performed for the rapidity and simplicity of operation. As the target, the detection limit of prostate-specific antigen (PSA) was 15.66 pg/mL in our designed biosensor. Besides, a good linear relationship was obtained. The designed biosensor demonstrated good specificity and successfully applied to clinical serum samples detection.

KEYWORDS: non-enzyme amplification, prostate-specific antigen, AgNPs dissolution, aggregation-induced emission, magnetic separation

The design and promotion of sensitive, portable and cost-effective platforms for disease-related biomarkers detection is extremely desirable in clinical research and early diagnosis.[1-3] Various significant detection platforms based on enzyme-catalyzed signal amplification have been reported, such as electrochemical,[4-5] chemiluminescence,[6-7] raman,[8-9] fluorescence[10-11] and colorimetric assays.[12-13] Currently, the immunofluorescence assay was recognized as the most widely applied method, which could well accommodate with immune sandwich reaction and coupled with considerable sensitivity.[14] However, the inherent defects of enzymes include poor stability, volatile activity, and high-cost, seriously undermine the enzyme-based performance and curb their wide application.[15-16] Therefore, there is still a compelling demand for novel enzyme-free biosensors with high sensitivity, operational simplicity for biomarkers detection.

In recent years, the advancements in nanomaterials open new ways for non-enzyme bio-detection. Especially the noble metal nanoparticles, showing good biocompatibility,[17]

large extinction coefficient,[18] and unusual chemical properties,[19] have been successfully employed in medical testing and chemical analysis fields. Gold nanoparticles, CuS nanoparticles, and ZnO quantum dots have been performed as fluorescent signal converters by anchoring on antibodies for biomarkers detection,[20-22] but without other accessional signal amplification. Notably, the silver nanoparticles (AgNPs) have drawn great interests due to its remarkable AgNPs-to-Ag^+ signal amplification characteristic by chemical etching. Moreover, the Ag^+ has been widely used in bioanalytical sensors for ions,[23] proteins,[24] small molecule,[25] and nucleic acid[26] detection due to its unusual electronic and chemical properties. Hydrogen peroxide (H_2O_2), as the potent oxidative etchant, can instant etch the AgNPs and convert atoms into ions due to the higher electrochemical potential than Ag^+/Ag. [27] And according to the report,[28] one 20 nm AgNPs can be dissolved into probably 2×10^5 of Ag^+, which can endow the testing system with another effective signal magnification. Considering that the AgNPs-to-Ag^+ signal enhancement strategy initiated by AgNPs has rarely been reported in fluorescent immunoassays, we are inspired for further explorations.

Lately, the aggregation-induced emission (AIE) has shown good application prospects owing to the significant advantages in bioanalyte sensing with photobleaching resistance and fluorescent enhancement.[29-30] As we all know, the traditional fluorescent dyes often exhibit the effect of aggregation-caused quenching (ACQ), which will seriously compromise the sensitivity.[31-32] Unlike the traditional fluorophores, AIE macromolecules with flexible structures of low-frequency torsional motions have almost no fluorescence in solution, but exhibit enhanced emission in aggregated pattern, promoting a superior fluorescent turn-on detection platform.[33-34] Based on the AIEgen, specific fluorogenic Ag^+-induced aggregation strategy was proposed. And a novel AIEgen TPE-4TA was designed and synthesized by Tang's team for innovative fluorescence bio-silver staining assay that could substitute for the traditional silver nitrate staining. The novel silver attaining by AIE aggregation luminescence could overcome the traditional method defects, enhance silver staining effect and achieve sensitive polyacrylamide gels imaging and detection.[35] Considering the advantage of AIEgens, the specific fluorogenic Ag^+-TPE-4TA aggregation strategy was also used in our designed detection system.

Herein, we proposed a novel enzyme-free fluorescent biosensor with significant cascade amplification based on effective AgNPs-to-Ag^+ etching sensitization and specific fluorogenic Ag^+-TPE-4TA aggregation. In this work, the proposed biosensor was evaluated by the selected biomarker-prostate-specific antigen (PSA). The PSA specific antibody were respectively immobilized on the surface of MBs and AgNPs for MB-Ab1 and AgNPs-Ab2 probes preparation. The AgNPs-Ab2 probes can attache on the surface of MBs by sandwich immune response via target PSA. The immune-complex was collected by magnetic separation. Each AgNP would undergo effective etching by H_2O_2 and dissolved into thousands of Ag^+, which endowed the designed biosensor with desirable sensitivity. Meanwhile, the released Ag^+ could specifically turn on the fluorogenic Ag^+-TPE-4TA aggregate as a specific switch based on Ag^+ and 4TA precipitate reaction, striving to enhance the performance of specificity and selectivity with low background signal. And the adoption of immunomagnetic beads with superior performances, ensuring the efficient separation and facile operation of the assay. Overall, this non-enzyme amplification biosensor achieved ideal convenience, cost-effective, high sensitivity and excellent stability in protein biomarkers detection. It could overcome the defects of enzymes and broaden the application of aggregation-induced luminescence, providing a robust tool in clinical early disease diagnosis.

Methods

Materials

Carboxyl modified magnetic nanoparticles (MBs, 200 μM in diameter) were purchased from BaseLine (Tianjin, China). Prostate-specific antigen (PSA) and capture antibody Ab1 (anti-mouse polyclonal antibody, IgG1), labeled antibody Ab2 (anti-mouse monoclonal antibody, IgG2a), anti-mouse secondary antibody, carcino-embryonic antigen (CEA), carbohydrate 153 antigen (CA-153), and human chorionic gonadotropin antigen (HCG) were supported by Bioscience (Tianjin, China). Human serum albumin (HAS), ovalbumin (OVA) and bovine serum albumin (BSA) were acquired from Solarbio (Beijing, China). Sodium borohydride ($NaBH_4$) was provided by Aladdin (Shanghai, China). Silver nitrate ($AgNO_3$) and trisodium citrate were obtained from Sigma-Aldrich. Hydrogen peroxide (H_2O_2) was purchased from Aladdin (Shanghai, China). Hydrochloric

acid (HCl) was supported by Nanjing Reagent (Nanjing, China). The fluorescence intensity of Ag^+-TPE-4TA was detected by microplate reader (Infinite M200pro, Techan, Switzerland) at the excitation wavelength of 368 nm.

Preparation of 4 nm silver seeds and 20 nm AgNPs

The silver seeds (4 nm) and $AgNP_S$ (20 nm) were prepared by the reported method.[36] The silver seeds of 4 nm-diameter were synthesized firstly. Briefly, sodium citrate (1% w/v, 10 mL) and ddH_2O (37.5 mL) were mixed in the three-necked flask and heated to 70℃. After that, 0.85 mL of $AgNO_3$ (1% w/v) and 1 mL of $NaBH_4$ (0.1% w/v) were added immediately with stirring at 70℃ for 1 h. Thereafter, the solution of 4 nm silver seeds was stored at 4℃ in dark for further synthesis of 20 nm AgNPs.

For the synthesis of 20 nm AgNPs, the sodium citrate (1% w/v, 1 mL) and ddH_2O (37.5 mL) were heated boiling for 15 minutes firstly. Next, 5 mL of above 4 nm-diameter silver seeds solution was added in the mixture, then add 0.85 mL of $AgNO_3$ (1% w/v) solution. Continuous stirring for 60 min. The AgNPs solution (20 nm) was stored at 4℃ in dark for subsequent assays after centrifuged and redistributed in ddH_2O. The size of silver seeds and AgNPs was both observed. The absorbance of particles was recorded by the Nanodrop.

Preparation of MBs-Ab1 probes

At first, the carboxylated MBs (5 mg/mL, 100 μL) were washed twice with 500μL MEST (10 Mm MES, PH 6.0, 0.05% Tween-20). Then, EDC (5 mg/mL, 200 μL) and NHS (5 mg/mL, 200 μL) were added for carboxyl activation with 30 min, remove the MEST supernatant by magnetic separation and resuspended in PBS. 10 μL of capture antibody (Ab1, 5.1 mg/mL) was added and incubated for 3 h. Then MBs-Ab1 probes were blocked by BSA (10 mg/mL). Finally, washed with PBST (0.05% Tween-20, PH=7.4) by magnetic separation, and then resuspended in PBST (PH 7.4, 0.02% NaN_3, 0.5% BSA). The prepared MBs-Ab2 probes were stored at 4℃ for the following assays.

Preparation of $AgNP_S$-Ab2 probes

First, K_2CO_3 (0.2 M, 20 μL) was added into 1 mL of AgNPs (20 nm), for adjusting the pH to approximately 8.0. Then, mixed with labeled detection antibody (Ab2, 1 mg/mL, 10 μL) for 2 h. After that, the BSA solution (10 mg/mL, 100 μL) was added for another incubation of 1 h. Then, the mixture was washed three times by 1% BSA. Finally,

the $AgNP_S$-Ab1 probes stored at 4℃ in dark with 500 μL PBST (1% BSA, 0.05% Tween-20) for further experiments.

Fabrication of immunochromatographic test strip

The test strip includes four parts: three pads and one reaction member (test line (T line), control line (C line)). Firstly, the anti-mouse secondary antibody (1.5 mg/mL) was fixed to the film for C line. The Ab1 (1.5 mg/mL) was dispensed on T line for PSA signal readout. As for the control and test group of the immunoassay, 4 μL of tenfold concentrated AgNPs-Ab2 probes was mixed and incubated with 36 μL of PBS and 36 μL of target PSA (1 μg/mL) for 20 min, respectively. Then, the mixture (40 μL) was taken for testing. The signal can be read out within 5 min.

Fluorogenic Ag^+-Tetrazolate (Ag^+-TPE-4TA) aggregation

The TPE-4TA was dissolved in water solution with a final concentration of 5 μM, and adjust the PH to 8.0 for increasing the solubility with weakly invisible fluorescence. Then, a range of different concentrations of silver ions (1 μL) was added, and recorded immediately by the UV-vis and fluorescence spectrophotometer. Further, 50 μL of 20 μM of different ion solution (Ag^+, Na^+, K^+, Mg^{2+}, Ca^{2+}, Fe^{3+}) was reacted with 150 μL of TPE-4TA solution, and the fluorogenic Ag^+-TPE-4TA was studied for ion specificity. In addition, different concentrations of TPE-4TA (in the range of 5 to 40 μM) were studied by aggregated with Ag^+ solution.

AgNPs Etching by H_2O_2

To test the process and efficiency of etching, 50 μL AgNPs was incubated with 10 μL H_2O_2 (30%) compared with 10 μL ddH_2O at 37℃ for 20 min, and the absorbance was detected by UV-vis. Then, 150 μL TPE-4TA was added for testing the etching efficiency and fluorogenic aggregation by fluorescence analysis. What's more, the etching process and fluorogenic aggregation were also studied by treatment with a series of H_2O_2: 0%, 5%, 10%, 15%, 20%, 25%, and 30% of 10 μL.

Non-enzyme cascaded amplification assay of PSA

At first, the admixture of MBs-Ab1 probes (10 μg) and target PSA (50 μL) was shaken at 37℃ for 1 h. Next, 50 μL of AgNPs-Ab2 probe was added for continue incubation at 37℃ for 1 h. Subsequent the effective magnetic separation with washing buffer (PBS, 0.05% Tween-20). After that, 50 μL of ddH_2O and 10 μL of H_2O_2 (10%)

was added, followed by etching for 30 min at 37℃. Finally, 150 μL of TPE-4TA (5 μM, PH 8.0) was added. The fluorogenic Ag^+-TPE-4TA intensity was recorded by a microplate reader.

Optimization test

To get the optimal detection conditions, the etching efficiency and probes dosage were optimized. 10% H_2O_2 was used for the etching of AgNPs-Ab2 probes according to the above results. We first studied the etching time. 50 μL of AgNPs-Ab2 probes was incubated with 10 μL of H_2O_2 at 37℃ for 0, 5, 10, 20, 30 min, respectively. Then the etching temperature was also optimized. 50 μL of AgNPs-Ab2 probes was dissolved by H_2O_2 for 30 min at different temperature (4℃, 25℃, 37℃, 45℃), respectively. The value of UV-vis absorption was recorded for etching efficiency evaluation. Next, we optimized the amounts of Ab2 for AgNPs-Ab2 probes preparation. The final detection signals were recorded respectively after the treatment with AgNPs-Ab2 probes with amounts of Ab2: 2.5, 5, 10, 15, 20 μL of 5.1 mg/mL. Further, the amounts of MBs-Ab1 probes were also optimized. The PSA was detected by 2, 4, 6, 8, 10 μg of prepared MBs-Ab1 probes.

Specificity evaluation

The specificity evaluation of the detection biosensor was performed with specific target PSA and other non-specific antigens and proteins (HCG, CEA, CA-153, BSA, OVA, HSA). According to the above reaction steps of Ag^+-TPE-4TA-based immunoassay for PSA detection, 50 μL of specific target PSA and non-specific proteins was applied to the immunological assay. After the Ag^+-TPE-4TA aggregation-induced luminescence, the fluorescence intensity was recorded by a microplate reader.

Clinical serum samples detection

The adaptability of the biosensor for clinical serum samples testing was performed by standard addition method. In brief, PSA standard was diluted by serum to prepare samples with various concentrations, and the fluorescence value was detected by the designed biosensor. The linear equation was obtained by plotting the ΔF versus PSA concentrations. Then to test the universality, different healthy serum was used to prepare PSA samples with same final concentration (100 pg/mL). Finally, according to the standard curve, the detected values detected by the biosensor were compared with the theoretically added values. Then, a range of PSA concentrations (50, 120, 200, 250, 300

pg/mL) were diluted by the same serum. The corresponding content and recovery were also detected.

Results and discussion

Mechanism of the non-enzyme amplification biosensor

In this work, a novel non-enzyme amplification biosensor was carried out. The working principle was shown in scheme 1. The specific antibody Ab1 and Ab2 were respectively immobilized on the surfaces of MBs and AgNPs for MB-Ab1 and AgNPs-Ab2 probes preparation. Through the robust chemical decomposition of AgNPs, the subsequent aggregation-induced emission was integrated into the detection biosensor. By using the high-performance magnetic beads, the efficient separation would help to improve the facile operation. As shown in the following, in the presence of specific antigen, the AgNPs-Ab2 could be captured through sandwich-type immunoreaction and enriched on the surface of MB-Ab1, and the uncaptured ones would be washed away by the "one-step" efficient magnetic separation. As the efficacious etchant for Ag^+, the oxidant H_2O_2 could dissolve the AgNPs of MB-Ab1-antigen-AgNPs-Ab2 sandwich-type complex, resulting in numerous Ag^+ for specific fluorogenic Ag^+-TPE-4TA aggregation with low background and significant signal enhancement. Overall, though this AgNPs-to-Ag^+ and metal-linked amplification, this non-enzyme cascaded amplification biosensor was constructed for protein biomarkers quantitative detection with high sensitivity and specificity.

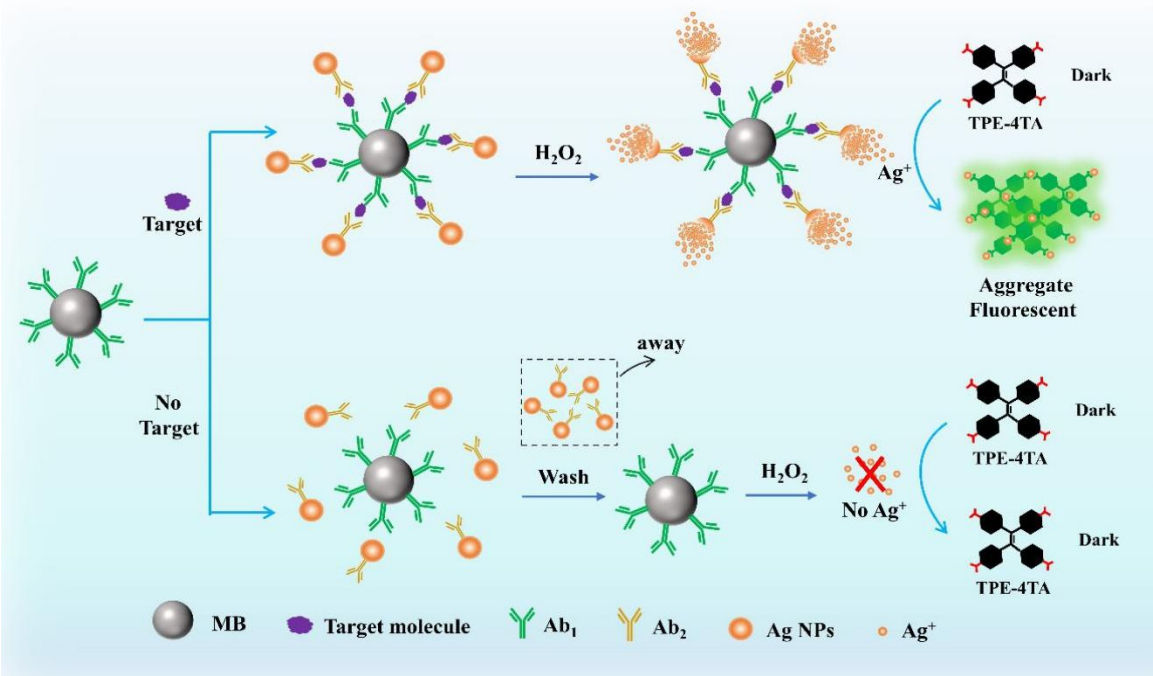

Scheme 1. Schematic illustration of the non-enzyme amplification biosensor based on effective AgNPs-to-Ag^+ etching sensitization and fluorogenic Ag^+-tetrazolate aggregation for protein biomarkers detection.

Morphological characterization of nanoparticles

The AgNPs (4 nm) were synthesized as starter seeds by $NaBH_4$ reduction principle. The morphological characterization was verified by surface plasmon resonance (SPR) firstly. As known from Figure 1b, the starter seeds solution presented a brighter brownish yellow with 391 nm absorption peak, which was similar to the SPR spectra of silver nanoparticles as reported. Then, the one-step starter seeded growth of AgNPs (20 nm) were obtained (Figure 1a). The optical UV-vis spectra of nanoparticles were determined by SPR, depending on the size and shape of synthesized AgNPs. Contrasted with figure 1a, the solution of 20 nm AgNPs exhibited a deeper brownish yellow, and the sharp SPR extinction also had a slight red shift to 400 nm (Figure 1c). Furthermore, evaluated by the TEM and dynamic light scattering, the resulting 20 nm AgNPs with uniform size and well dispersed (Figure 1d, 1e).

Then, the Ab2 was coupled to AgNPs for the preparation of detection AgNPs-Ab2 probes. Figure S2a exhibits the UV-vis of Ab2 protein, pure AgNPs and Ab2 modified AgNPs. Consistent with the protein-specific absorption value, Ab2 showed maximum

absorbance at the wavelength of 280 nm. As individual nanoparticles, the obtained AgNPs exhibited the characteristic strong plasmon absorption peak at 400 nm. It is clear that the absorption peak of forming AgNPs-Ab2 had a modest redshift from 393 nm to 400 nm compared with pure AgNPs. This redshift of forming AgNPs-Ab2 probes was attributed to the modification of Ab2 that caused the dielectric property changes of AgNPs.

To validate the biological activity of Ab2 modified on AgNPs, we took the immunochromatographic test strip for determination. Like the characteristics of gold nanoparticles, the aggregation of AgNPs on the T or C line also leads to the appearance of obvious signal bands. As shown in Figure S2b, based on the Ab2-second antibody immune response, there is only an obvious band of C line appeared when just adding the AgNPs-Ab2 probes without target PSA. However, after the incubation with target PSA, the AgNPs-Ab2-PSA mixture could be captured by the Ab1 sprayed at the T line. So, the obvious bands of T and C lines were both observed. The results confirmed that the formed AgNPs-Ab2 probe still maintained good biological activity and could be used in subsequent immunoassays.

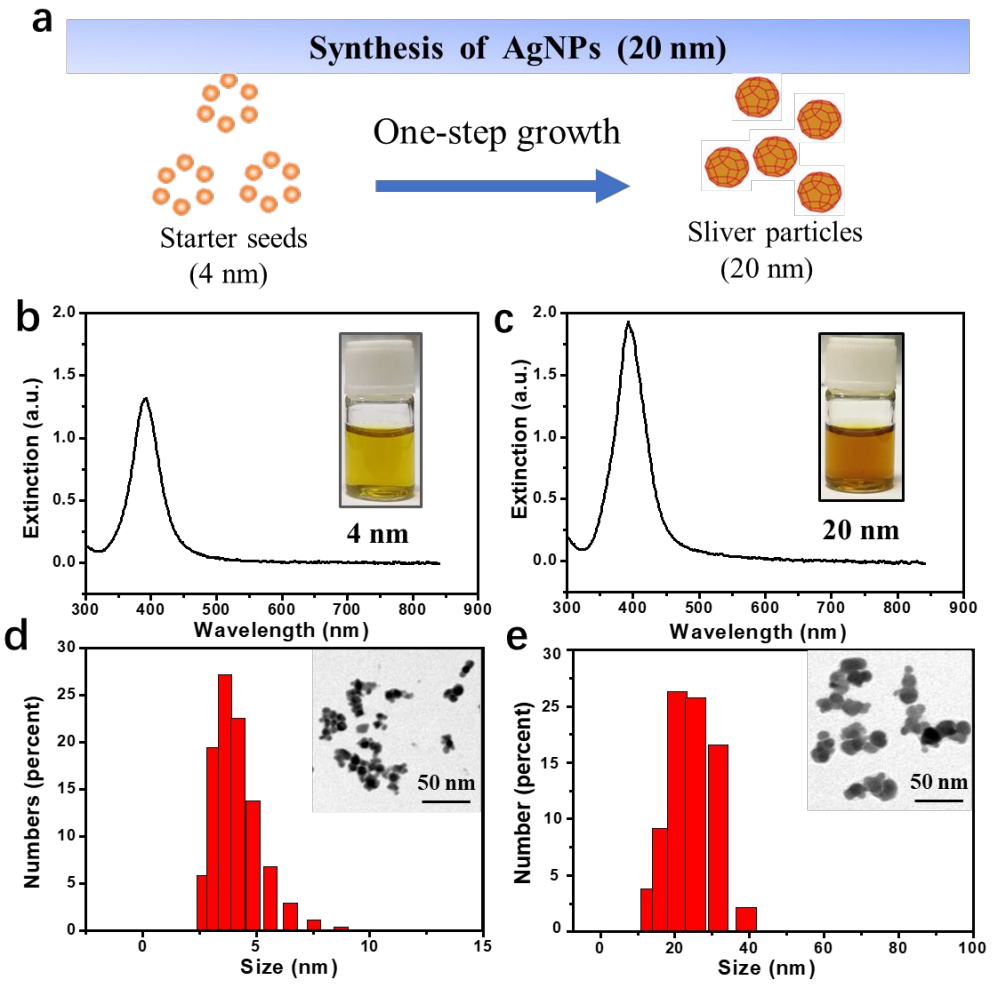

Figure 1. (a) Synthesis of 20 nm silver nanoparticles by one-step growth of starter seeds (4 nm). (b) UV-vis characterization of the silver seeds (4 nm). Inside: the corresponding digital picture. (c) UV-vis characterization of the AgNPs (20 nm). Inside: the corresponding digital picture. (d, e) Dynamic light scattering (DLS) of the 4 nm silver seeds and 20 nm AgNPs. Inside: TEM image characterization.

Aggregation induced luminescence based on fluorogenic Ag^+-Tetrazolate

Inspired by the novel aggregation-induced luminescence, the fluorogenic visualization was triggered by the specific Ag^+ inducer and designed AIE dyes. In this work, as the infinite metal-coordination polymers for Ag^+, the new type of water-soluble AIE material TPE-4TA was designed and synthesized by our team as reported before,[35] and the NMR characterization was shown in Figure S1. It was designed with Ag^+-specific targeting 1/2H-tetrazole compounds (4TA) and aggregation-induced fluorescence TPE

core. The designed 4TA compounds can specifically capture and precipitate out Ag^+ to induce aggregation, which limited the rotation of TPE core and endowed the Ag^+-tetrazolate aggregation-induced luminescence. Contrary to the traditional fluorescent dyes, the TPE-4TA has weak fluorescence in dissolved solution, but it emits strongly at 504 nm in Ag^+-Tetrazolate aggregated complex. In Figure 2a, the TPE-4TA emits faintly in deionized water when not aggregated, and it has no-fluorescence due to the flexible TPE core structure. As expected, Ag^+ could specifically turn on the fluorescence of TEP-4TA aggregated complex instantly. Indeed, the fluorescence emission at 504 nm was enhanced gradually by the stepwise addition of Ag^+ because of the restricted free rotation. By evaluating the fluorescence intensity of TEP-4TA (5 μM) with different amounts of Ag^+, a good linear regression (R^2=0.99227) from 0 to 100 nM was established (Figure S3). And the calculated detection limit of Ag^+ was 0.43 nM, which is more sensitive than the optimum fluorometric assay. In addition, the interference of other metal ions on the fluorogenic sensing was also explored. In the previous silver staining assay,[35] the effect of silver ions and interference of a number of cations on TPE-4TA AIE were studied in phosphate buffer. The results showed that there is no fluorogenic response was detected with other ions at the PH**>**8. As shown in Figure 2c, at PH>8, the metal ions could not turn on the fluorescence except Ag^+, proving the highly specific of the fluorogenic sensing, which was consistent with the previous reports. To get the lowest background signal of the fluorogenic sensing, the concentration of TPE-4TA was also investigated (Figure 2d). Excess Ag^+ was mixed with different amounts of TPE-4TA individually. With a further increase of TPE-4TA, the fluorogenic sensing exhibited an equivalent fluorescence intensity with the little discrepancy, while coupled with a gradual enhancement of TPE-4TA autofluorescence because of the solubility. So, considering the background signal, the low concentration of TPE-4TA (5 μM) was performed for the fluorogenic Ag^+ detection in the subsequent assays.

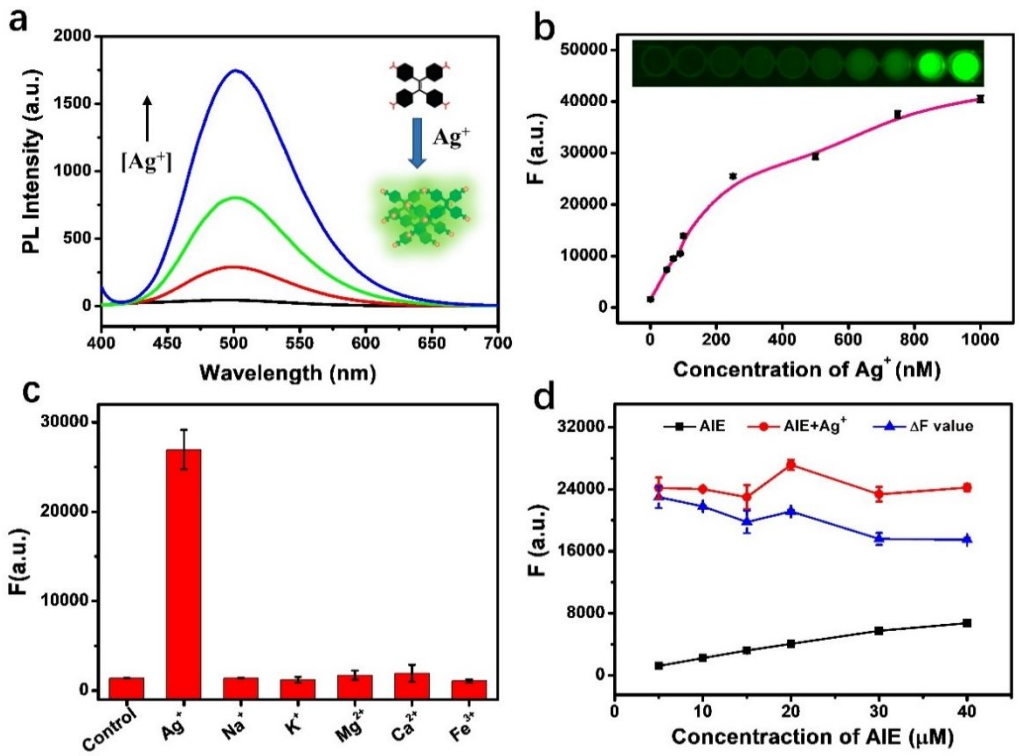

Figure 2. Ag^+-Tetrazolate aggregation-induced fluorogenic process. (a) Fluorescence spectrum of TPE-4TA based on fluorogenic aggregation by different concentrations of Ag^+ inducer. (b) Plotting of fluorescence intensity at 504 nm with Ag^+ inducer. Inside: corresponding fluorescent images recorded by the Nanodrop. (c) Characterization of the Ag^+-tetrazolate aggregation specificity. The fluorescence emission at 504 nm was evaluated by the reaction of TPE-4TA with various metal ions: Ag^+, Na^+, k^+, Mg^{2+}, Ca^{2+}, Fe^{3+} in deionized water. (d) Background signal evaluation of fluorogenic sensing. Comparison of the fluorescent Ag^+-tetrazolate aggregate by mixed with various concentrations of TPE-4TA and Ag^+.

Effective AgNPs-to-Ag^+ etching sensitization

As the powerful oxidizing agent and effective etchant, H_2O_2 was introduced for AgNPs etching. According to the reports, each 20 nm AgNP contains approximately 2×10^5 Ag atoms, which can be easily released in individual Ag^+ status by H_2O_2 etching. The etching process was inspected by the UV-vis spectrum. In Figure 3a, the pure AgNPs exhibited a sharp SPR peak at 400 nm, but it dropped sharply and disappeared instantly in the addition of excess H_2O_2. It can be seen that AgNPs can be effectively dissolved into Ag atoms and completely released in the form of Ag^+. What's more, a range of different H_2O_2 concentrations (0%, 5%, 10%, 15%, 20%, 25%, 30%) were used for evaluation and

optimization of AgNPs etching efficiency. Figure 3c showed that the corresponding absorption peaks of AgNPs were gradually decreased from 0.377 to 0.174, 0.081, 0.057, 0.06, 0.039, and 0.038 with the increasing concentration of H_2O_2. By calculation, the etching efficiency basically reached a plateau when the concentration of H_2O_2 was 10%. As a result, we choose 10% H_2O_2 for AgNPs etching.

Further, in order to demonstrate the feasibility of non-enzyme signal amplification, we verified that the Ag^+-TPE-4TA aggregation-induced luminescence can be achieved by thousands to millions Ag^+ caused by the disintegration of AgNPs. As illustrated in Figure 3b, the AgNPs and TPE-4TA mixture solution has no fluorescence under UV irradiation coupled with a negligible emission peak. It means that the pure AgNPs have no effect on the aggregation of TPE-4TA and the opening of fluorescence. After the addition of excess H_2O_2, the bright green fluorescence of Ag^+-TPE-4TA aggregation was opening immediately. The conspicuous peak was located at 504 nm, which is in agreement with the anterior resulting of Ag^+ and PTE-4TA reaction. It is no doubt that the rupture sensitization of AgNPs would contribute to higher sensitivity.

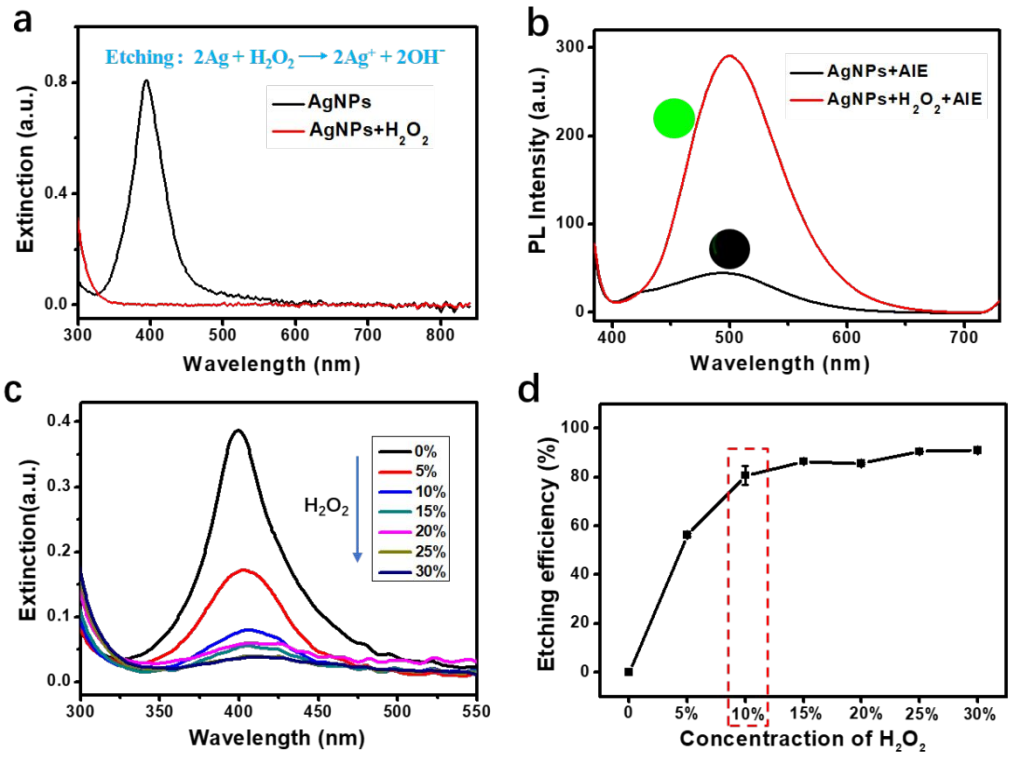

Figure 3. The non-enzyme signal amplification based on AgNPs etching by H_2O_2. (a) UV-vis spectrum of AgNPs before and after etching by H_2O_2. (b) The verification of fluorescent signal

amplification owing to the Ag^+ release initiated the aggregation-induced luminescence. (c, d) AgNPs etching efficiency evaluation and optimization: $AgNP_S$ were dissolved with different concentrations (0%, 5%, 10%, 15%, 20%, 25%, 30%) of H_2O_2.

Optimization test

The condition of AgNPs-Ab2 probes etching by H_2O_2 was optimized to obtain the great AgNPs-to-Ag^+ signal amplification. There is no doubt that the instantaneous dissolution of pure AgNPs and countless release of Ag^+ enabled an effective magnification.

But considering the wrapping and covering of Ab2 on the surface of AgNPs, the etching time and temperature of AgNPs-Ab2 probes need further exploration to achieve the great signal amplification in biomarker detection. As indicated by Figure 4a, due to the prolonged etching time, the absorbance of AgNPs-Ab2 probes decreased gradually at 400nm. According to the calculated etching efficiency, 30 min was founded to be the optical etching time with 10% H_2O_2 (Figure 4a). We then verified the temperature on AgNPs-Ab2 probes etching (Figure S4b). It can be seen that there is a lower etching efficiency when incubated at 4℃ or 25℃. But we can get an ideal etching effect at 37℃ that almost identical to the case of 45℃ (Figure 4b). Herein, we adopt 10% H_2O_2, 30 min and 37℃ as the optimal etching factors for the biomarker detection.

In addition, the dosage of probes was also optimized for immune assays. We first studied the amounts of MBs-Ab1 probes. As illustrated in Figure 4c, the change value of fluorescence relative to the control (ΔF) was increased in the range of 0 to 6 μg MBs-Ab1 probes. And attributed to the thoroughly capture of target antigen by Ab1, we can get the maximum ΔF when added 6 μg of MBs-Ab1 probes. The excess antibody may affect the formation of immune complexes or increase background signal, so more MBs-Ab1 probes caused the decrease of ΔF. Overall, 6 μg of MBs-Ab1 probes was carried out as the optimal amount in biomarker detection. Meanwhile, the concentration of Ab2 on AgNPs-Ab2 probes was also optimized (Figure 4d). On one hand, less antibody will affect the stability of probes, One the other hand, more antibody will affect the immune assay. When modified with 10 μg Ab2, the stable AgNPs-Ab2 probes can be acquired with the ideal detection ΔF value. Thus, 10 μg of Ab2 was regarded as the best factor in this assay.

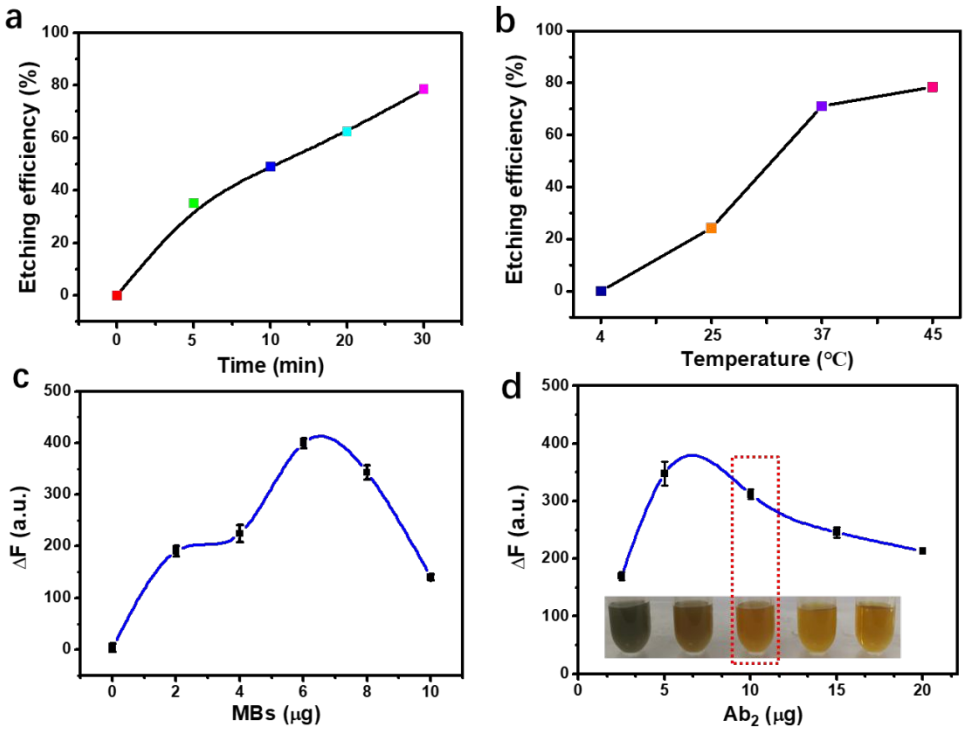

Figure 4. Optimization test. (a) The analysis of the most effective etching time for AgNPs-Ab2 probes. (b) The analysis of the best etching time for AgNPs-Ab2 probes. The assays were performed by etching 50 μL solution of AgNPs-Ab2 probes with 10 μL of H_2O_2 (10%). (c) Optimization of the optimal amount of MBs for target detection. (d) Optimization of the best Ab2 concentration for AgNPs-Ab1 probes preparation of the target detection.

Sensitivity and specificity of PSA detection

Based on the AgNPs-to-Ag^+ and metal-linked Ag^+-TPE-4TA amplification, low consistence of target antigen can bring clear fluorescence signal, contributing to a significant enhancement for biomarker detection. As for the non-enzyme amplification fluorogenic sensing, PSA biomarker was chosen as the detection target to evaluate the sensitivity. As displayed in Figure 5a, a strong PSA-dependent ΔF value was observed, suggesting that more Ag^+ released and fluorescent Ag^+-TPE-4TA generated due to the increased target PSA. Moreover, it showed a quality linear relationship (R^2 = 0.98236) between the ΔF value and PSA concentrations (10 to 250 pg/mL). The detection limit (LOD) was 15.66 pg/mL. To further ensure the specificity and selectivity, identical to the specific target PSA detection described above, we tested other non-specific proteins

(HCG, CEA, CA-153, BSA, HAS, OVA) for the sandwich immunoassays. As can be seen from Figure 5b, a strong ΔF value was only obtained for specific PSA biomarker, showing the high specificity and selectivity.

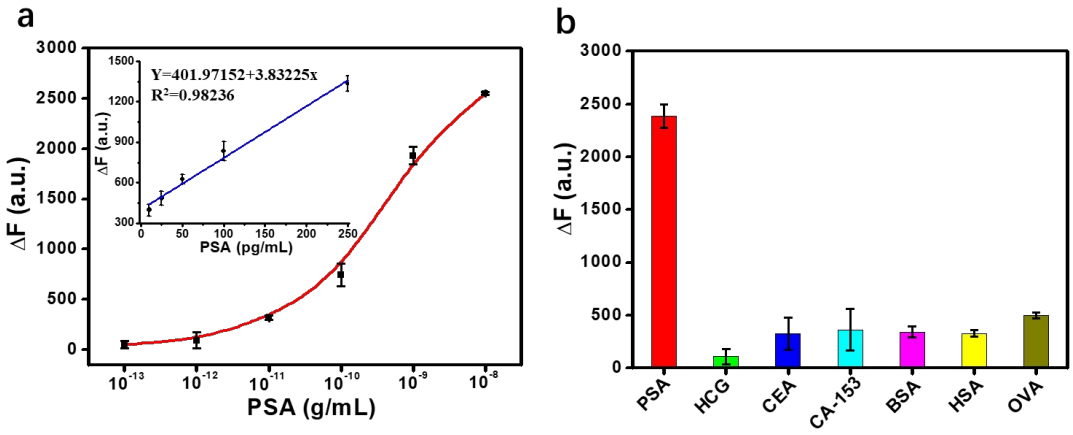

Figure 5. Sensitivity and selectivity evaluation of the proposed sensing. (a) The corresponding fluorescence detection with versus different amounts of target PSA. Inside: calibration curve for PSA detection by the designed biosensor. (b) The specificity and selectivity of the biosensor toward various antigens and proteins: PSA, HCG, CEA, CA-153, BSA, HAS, and OVA. The concentration of each protein was 1 ng/mL.

Clinical samples diagnosis

This non-enzyme amplification biosensor was also assessed in terms of accuracy and practicability with standard addition method from spiked human serum samples as the previous reports.[37-38] Firstly, different amounts of PSA standards were prepared by serum samples. A positive linear response between target PSA (from 50 to 500 pg/mL) and ΔF was acquired (R^2 = 0.9974, Figure 6a). Then, the same certain amount of PSA standard was added into seven different healthy human serum samples with the final concentration of 100 pg/mL, and a good agreement between spiked and detected concentrations was obtained for the qualification of PSA (Figure 6b). Further, we also studied the theoretical and observed amount of PSA from the same healthy spiked serum samples by diluting PSA concentrations (from 50 to 300 pg/mL). As shown in Figure 6c, the observed and theoretical value was still maintained a good consistent, and the specific percent recovery was calculated from 82.3 % to 110.3 % (Figure 6d), indicating the applicability for clinical samples detection.

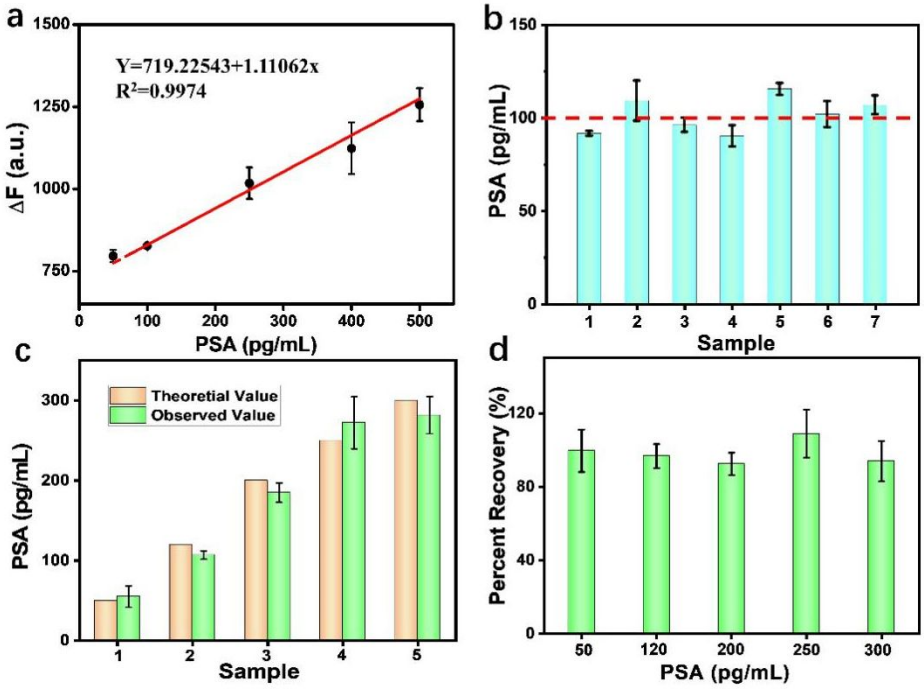

Figure 6. Serum samples diagnosis by the standard addition method. (a) Standard curve determination of the PSA standard samples. (b) Detection of PSA standard with the same concentration in different healthy serum. The PSA was picked into different healthy serum samples with the final concentration of 100 pg/mL. (c) Analysis of PSA standard with serious concentrations. The PSA standard with various concentrations (60, 120, 200, 250, 300 pg/mL) were spiked into the same serum sample. (d) Specific percent recovery of target PSA detection with standard addition method.

Conclusions

In conclusion, a novel non-enzyme amplification strategy based on fluorogenic Ag^+-tetrazolate aggregation was demonstrated for biomarkers detection. The significant cascade enhancement was achieved by the efficient AgNPs-to-Ag^+ dissolution amplification strategy and robust Ag^+-linked fluorogenic amplification strategy. Notably, such a cascade signal amplification strategy with non-enzyme was rarely reported. The cascade amplification technology was compatible with magnetic nanoparticles, making it straightforward to construct a more sensitive and reliable methodology. Thus, this detection method is capable of providing a promising platform in clinical diagnosis.

ASSOCIATED CONTENT

Supporting Information

Supporting Information Available: The following files are available free of charge.

NMR characterization of TPE-4TA; AgNPs-Ab2 probes performance evaluation; Calibration curve for Ag^+ detection; Optimization test; Table1 and Table 2 for the detection recoveries of standard PSA. Table 3 for the comparison with different non-enzyme methods.

Acknowledgments

The authors gratefully acknowledge financial support from the National Natural Science Foundation of China (31600800), National Natural Youth Foundation of China (21705118), the National Key Research and Development Plan "nanotech" key project (2017YFA0205104), and the Natural Science Foundation of Tianjin, China (17ZXMFSY00210, 16ZXMJSY00010, 17JCQNJC09100).

Conflict of interest

The authors declare no competing interest exists.

Reference:

(1) Kairdolf, B. A.; Qian, X. M.; Nie, S. M. Bioconjugated Nanoparticles for Biosensing, in Vivo Imaging, and Medical Diagnostics. *Anal. Chem.* **2017,** *89* (2), 1015-1031.

(2) Qin, Z. P.; Chan, W. C. W.; Boulware, D. R.; Akkin, T.; Butler, E. K.; Bischof, J. C. Significantly Improved Analytical Sensitivity of Lateral Flow Immunoassays by Using Thermal Contrast. *Angew. Chem., Int. Ed.* **2012,** *51* (18), 4358-4361.

(3) Yang, Q. H.; Gong, X. Q.; Song, T.; Yang, J. M.; Zhu, S. J.; Li, Y. H.; Cui, Y.; Li, Y. X.; Zhang, B. B.; Chang, J. Quantum dot-based immunochromatography test strip for rapid, quantitative and sensitive detection of alpha fetoprotein. *Biosens. Bioelectron.* **2011,** *30* (1), 145-150.

(4) Abellan-Llobregat, A.; Jeerapan, I.; Bandodkar, A.; Vidal, L.; Canals, A.; Wang, J.; Morallon, E. A stretchable and screen-printed electrochemical sensor for glucose determination in human perspiration. *Biosens. Bioelectron.* **2017,** *91*, 885-891.

(5) Akanda, M. R.; Aziz, M. A.; Jo, K.; Tamilavan, V.; Hyun, M. H.; Kim, S.; Yang, H. Optimization of phosphatase-and redox cycling-based immunosensors and its application to ultrasensitive detection of troponin I. *Anal. Chem.* **2011,** *83* (10), 3926-3933.

(6) Devi, R. V.; Doble, M.; Verma, R. S. Nanomaterials for early detection of cancer biomarker with special emphasis on gold nanoparticles in immunoassays/sensors. *Biosens. Bioelectron.* **2015,** *68*, 688-698.

(7) Lee, Y.; Kim, S. S.; Lee, J. H. Chemiluminescent dual-enzyme immunoassays capable of simultaneously quantifying carbohydrate antigen 19-9 and carcinoma embryonic antigen in a sample. *Anal. Chim. Acta.* **2019,** *1060*, 88-96.

(8) Yang, L.; Gao, M. X.; Zhan, L.; Gong, M.; Zhen, S. J.; Huang, C. Z. An enzyme-induced

Au@Ag core-shell nanoStructure used for an ultrasensitive surface-enhanced Raman scattering immunoassay of cancer biomarkers. *Nanoscale* **2017,** *9* (7), 2640-2645.

(9) Cheng, Z.; Choi, N.; Wang, R.; Lee, S.; Moon, K. C.; Yoon, S. Y.; Chen, L. X.; Choo, J. Simultaneous Detection of Dual Prostate Specific Antigens Using Surface-Enhanced Raman Scattering-Based Immunoassay for Accurate Diagnosis of Prostate Cancer. *Acs Nano* **2017,** *11* (5), 4926-4933.

(10) Sanjay, S. T.; Fu, G. L.; Dou, M. W.; Xu, F.; Liu, R. T.; Qi, H.; Li, X. J. Biomarker detection for disease diagnosis using cost-effective microfluidic platforms. *Analyst* **2015,** *140* (21), 7062-7081.

(11) Zhang, W. H.; Ma, W.; Long, Y. T. Redox-Mediated Indirect Fluorescence Immunoassay for the Detection of Disease Biomarkers Using Dopamine-Functionalized Quantum Dots. *Anal. Chem.* **2016,** *88* (10), 5131-5136.

(12) Gao, Z. Q.; Hou, L.; Xu, M. D.; Tang, D. P. Enhanced Colorimetric Immunoassay Accompanying with Enzyme Cascade Amplification Strategy for Ultrasensitive Detection of Low-Abundance Protein. *Sci. Rep.* **2014,** *4*.

(13) Wei, W.; Zhang, C. Y.; Qian, J.; Liu, S. Q. Multianalyte immunoassay chip for detection of tumor markers by chemiluminescent and colorimetric methods. *Anal. Bioanal. Chem.* **2011,** *401* (10), 3269-3274.

(14) Chen, W.; Cai, S.; Ren, Q. Q.; Wen, W.; Zhao, Y. D. Recent advances in electrochemical sensing for hydrogen peroxide: a review. *Analyst* **2012,** *137* (1), 49-58.

(15) Zhao, H.; Zhang, C.; Crittle, T. D. Choline-based deep eutectic solvents for enzymatic preparation of biodiesel from soybean oil. *J. Mol. Catal. B:Enzym.* **2013,** *85-86*, 243-247.

(16) Xi, F. N.; Zhao, D. J.; Wang, X. W.; Chen, P. Non-enzymatic detection of hydrogen peroxide using a functionalized three-dimensional graphene electrode. *Electrochem. Commun.* **2013,** *26*, 81-84.

(17) Lu, R. Q.; Yang, D. P.; Cui, D. X.; Wang, Z. Y.; Guo, L. Egg white-mediated green synthesis of silver nanoparticles with excellent biocompatibility and enhanced radiation effects on cancer cells. *Int. J. Nanomed.* **2012,** *7*, 2101-2107.

(18) Chen, X. J.; Sanchez-Gaytan, B. L.; Qian, Z. X.; Park, S. J. Noble metal nanoparticles in DNA detection and delivery. *Wires. Nanomed. Nanobi.* **2012,** *4* (3), 273-290.

(19) Li, Y. X.; Chu, F. Q. Research on the Preparation of Silver Nanoparticles by Chemical Reduction Method. *Lect. Notes. Electr. En.* **2017,** *417*, 1109-1114.

(20) Ao, L. M.; Gao, F.; Pan, B. F.; He, R.; Cui, D. X. Fluoroimmunoassay for antigen based on fluorescence quenching signal of gold nanoparticles. *Anal. Chem.* **2006,** *78* (4), 1104-1106.

(21) Gu, B. X.; Xu, C. X.; Yang, C.; Liu, S. Q.; Wang, M. L. ZnO quantum dot labeled immunosensor for carbohydrate antigen 19-9. *Biosens. Bioelectron.* **2011,** *26* (5), 2720-2723.

(22) Zhu, Y. D.; Peng, J.; Jiang, L. P.; Zhu, J. J. Fluorescent immunosensor based on CuS nanoparticles for sensitive detection of cancer biomarker. *Analyst* **2014,** *139* (3), 649-655.

(23) Su, Y. T.; Lan, G. Y.; Chen, W. Y.; Chang, H. T. Detection of copper ions through recovery of the fluorescence of DNA-Templated copper/silver nanoclusters in the presence of mercaptopropionic. *Acid. Anal. Chem.* **2010,** *82* (20), 8566-8572.

(24) Xue, H. F.; Zheng, J. W.; Chen, Q. Y.; Wang, Q. S.; Lin, Y.; Chen, J. C. Ag^{+}-coordinated oligonucleotides on gold nanoparticles for anodic-stripping voltammetric immunoassay of cancer antigen 125 for cervical carcinoma. *Anal Methods-Uk* **2019,** *11* (23), 2976-2982.

(25) Chen, X.; Zhou, Y.; Peng, X. J.; Yoon, J. Fluorescent and colorimetric probes for detection of thiols. *Chem. Soc. Rev.* **2010,** *39* (6), 2120-2135.

(26) Zhang, J.; Liu, Y.; Zhi, X.; Zhang, C.; Liu, T. F.; Cui, D. DNA-templated silver nanoclusters locate microRNAs in the nuclei of gastric cancer cells. *Nanoscale* **2018,** *10* (23), 11079-11090.

(27) Zhang, Q.; Cobley, C. M.; Zeng, J.; Wen, L. P.; Chen, J. Y.; Xia, Y. N. Dissolving Ag from Au-Ag Alloy Nanoboxes with H2O2: A Method for Both Tailoring the Optical Properties and Measuring the H2O2 Concentration. *J. Phys. Chem. C.* **2010,** *114* (14), 6396-6400.

(28) Li, J. X.; Gao, Z. Q.; Ye, H. H.; Wan, S. L.; Pierce, M.; Tang, D. P.; Xia, X. H. A non-enzyme cascade amplification strategy for colorimetric assay of disease biomarkers. *Chem. Commun.* **2017,** *53* (65), 9055-9058.

(29) Chen, M.; Chen, R.; Shi, Y.; Wang, J. G.; Cheng, Y. H.; Li, Y.; Gao, X. D.; Yan, Y.; Sun, J. Z.;

Qin, A. J.; Kwok, R. T. K.; Lam, J. W. Y.; Tang, B. Z. Malonitrile-Functionalized Tetraphenylpyrazine: Aggregation-Induced Emission, Ratiometric Detection of Hydrogen Sulfide, and Mechanochromism. *Adv. Funct. Mater.* **2018,** *28* (6).

(30) Cheng, H. R.; Ji, Y.; Liu, F.; Lu, X. J. Rapid and visual detection for hypochlorite of an AIE enhanced fluorescence probe. *Luminescence* **2019**.

(31) Gao, H. Q.; Zhang, X. Y.; Chen, C.; Li, K.; Ding, D. Unity Makes Strength: How Aggregation-Induced Emission Luminogens Advance the Biomedical Field. *Adv. Biosyst.* **2018,** *2* (9).

(32) Li, X. Y.; Guo, X. D.; Cao, L. X.; Xun, Z. Q.; Wang, S. Q.; Li, S. Y.; Li, Y.; Yang, G. Q. Water-Soluble Triarylboron Compound for ATP Imaging In Vivo Using Analyte-Induced Finite Aggregation. *Angew. Chem., Int. Ed.* **2014,** *53* (30), 7809-7813.

(33) Zhang, X. Y.; Wang, K.; Liu, M. Y.; Zhang, X. Q.; Tao, L.; Chen, Y. W.; Wei, Y. Polymeric AIE-based nanoprobes for biomedical applications: recent advances and perspectives. *Nanoscale* **2015,** *7* (27), 11486-11508.

(34) Han, Z. G.; Yang, Z. F.; Sun, H. S.; Xu, Y. L.; Ma, X. F.; Shan, D. L.; Chen, J.; Huo, S. H.; Zhang, Z.; Du, P. Y.; Lu, X. Q. Electrochemiluminescence Platforms Based on Small Water-Insoluble Organic Molecules for Ultrasensitive Aqueous-Phase Detection. *Angew. Chem., Int. Ed.* **2019,** *58* (18), 5915-5919.

(35) Xie, S.; Wong, A. Y. H.; Kwok, R. T. K.; Li, Y.; Su, H.; Lam, J. W. Y.; Chen, S.; Tang, B. Z. Fluorogenic Ag(+) -Tetrazolate Aggregation Enables Efficient Fluorescent Biological Silver Staining. *Angew. Chem., Int. Ed.* **2018,** *57* (20), 5750-5753.

(36) Wan, Y.; Guo, Z. R.; Jiang, X. L.; Fang, K.; Lu, X.; Zhang, Y.; Gu, N. Quasi-spherical silver nanoparticles: Aqueous synthesis and size control by the seed-mediated Lee-Meisel method. *J. Colloid Interfsce Sci.* **2013,** *394*, 263-268.

(37) rturk, G.; Ozen, H.; Tumer, M. A.; Mattiasson, B.; Denizli, A. Microcontact imprinting based surface plasmon resonance (SPR) biosensor for real-time and ultrasensitive detection of prostate specific antigen (PSA) from clinical samples. *Sensor. Actuat, B* **2016,** *224*, 823-832.

(38) Wei, Q.; Zhao, Y. F.; Xu, C. X.; Wu, D.; Cai, Y. Y.; He, J.; Li, H.; Du, B.; Yang, M. H. Nanoporous gold film based immunosensor for label-free detection of cancer biomarker. *Biosens. Bioelectron.* **2011,** *26* (8), 3714-3718.

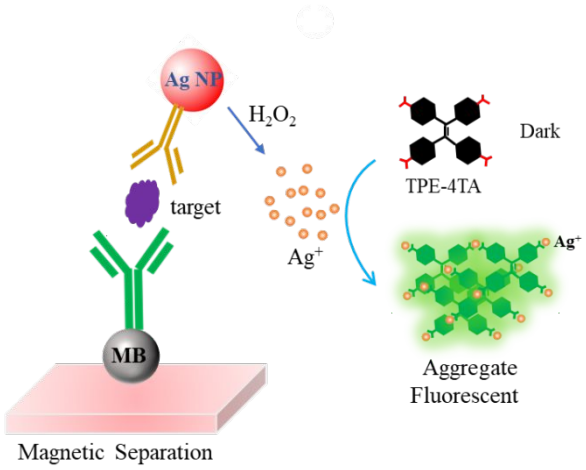
Ag NP
H_2O_2
Dark
TPE-4TA
target
Ag^+
Ag^+
MB
Aggregate
Fluorescent
Magnetic Separation

For TOC only